applied sciences

MDPI

Article

Dynamic Analysis and Parameter Optimization of the Cutting System for Castor Harvester Picking Devices

Fanting Kong [1,2], Defu Wang [1,3,*], Lei Shi [2], Huinan Huang [3], Qing Xie [2], Teng Wu [2], Yongfei Sun [2] and Changlin Chen [2]

[1] College of Engineering, Northeast Agricultural University, Harbin 150030, China
[2] Nanjing Institute of Agricultural Mechanization, Ministry of Agriculture and Rural Affairs, Nanjing 210014, China
[3] College of Mechanical and Electrical Engineering, Henan Agricultural University, Zhengzhou 450046, China
* Correspondence: dfwang640203@163.com

Abstract: Our study aimed to identify a design which would reduce cutting resistance during the harvesting of castor. This paper presents a theoretical study of the wave-type disc cutter, which plays an important role in castor harvesting. Based on the SPH–FEM coupling algorithm, a combined orthogonal rotation experiment was performed to study the effects of disc cutter thickness, edge angle, disc cutter rotation speed, and feeding speed on the maximum cutting force. The response surface method was used to achieve an optimal combination of all the test factors. Mathematical modeling of the maximum cutting force and influencing factors was utilized to obtain the optimal parameters for a cutting system consisting of wave-type disc cutters. The optimal results were obtained with a computer-simulated disc cutter rotation speed of 844.2–942.1 r/min, a feeding speed of 0.89–1.01 m/s, a disc cutter thickness of 2.71–3.15 mm, and an edge angle of 29.2–33.9°. Under these conditions, the maximum cutting force was less than 50 N. Finally, the experimental data and numerical computer simulation results were compared using cutting performance test verification. The analysis found that the test results and simulation results were largely consistent. Therefore, the simulation model was judged to be effective and reasonable.

Keywords: agricultural machinery; castor harvester; cutting system; SPH–FEM coupling method; cutting force; parameter optimization

check for updates

Citation: Kong, F.; Wang, D.; Shi, L.; Huang, H.; Xie, Q.; Wu, T.; Sun, Y.; Chen, C. Dynamic Analysis and Parameter Optimization of the Cutting System for Castor Harvester Picking Devices. *Appl. Sci.* **2023**, *13*, 2116. https://doi.org/10.3390/app13042116

Academic Editors: Mark J. Jackson and Roberto Romaniello

Received: 16 December 2022
Revised: 26 December 2022
Accepted: 31 December 2022
Published: 7 February 2023

Copyright: © 2023 by the authors. Licensee MDPI, Basel, Switzerland. This article is an open access article distributed under the terms and conditions of the Creative Commons Attribution (CC BY) license (https://creativecommons.org/licenses/by/4.0/).

1. Introduction

Castor is a common crop, well known for its specific oil, which is widely used in the chemical industry [1]. In addition, many castor extracts have significant pharmacological activities [2,3]. Because the castor plant places low demands on the growing environment and is simple to plant, with low input costs and high economic benefits, it is an important cash crop that enables farmers to increase their income. Castor production in India, China, Brazil, and Mozambique accounts for nearly 88% of world production [4,5]. The key restriction of castor production is the largely manual harvesting required. Mechanized harvesting is an effective way to promote the development of the castor industry and it is, therefore, necessary to study castor harvesting technology in order to solve the mechanization challenges, reduce the harvesting costs, and drive the sustainable development of the castor industry.

In recent years, scholars have designed and tested many types of castor harvester. Wu et al. [6] designed a castor harvesting device that used a set of wheel-saw cutters to cut the main stalk and then transport it to the thresh rollers by means of an entanglement device. The test showed that the castor harvester achieved the designed functions, but the harvesting ratio was 67.1 ± 6.8%, indicating that the harvester still required improvement. Liu et al. [7] developed the 4BZ-4 self-propelled castor harvester and performed technical research in terms of the physical characteristics and harvesting process of castor beans.

Stefanoni et al. [8] compared the effectiveness, machinery performance, and seed loss from the impact and cleaning systems of two combine harvesters equipped with a sunflower header and a cereal header, respectively, for harvesting castor beans. They observed that a disc cutter was more suitable for use in cutting systems for castor picking and that the structure of castor harvesters with disc cutters was much simpler than other types of cutting system, making it easier to automate castor harvesting. In the process of cutting, friction and wear between the cutter and the crops, soil, and, in particular, stone debris may lead to blade passivation and reduced cutting performance. Rostek et al. [9] studied the relationship between cutter life and the bending strength, ductility, and wear resistance of matrix materials. Song et al. [10] carried out a series of studies concerning tool self-sharpening technology. Momin et al. [11] established evaluation indexes, such as root damage degree, residual height, and blade quality change, and evaluated the cutting performance of cutters with different structural forms and surface treatment processes. In terms of material properties, it was recommended that the hardness of the quenched zone should be 48-60HRC and that the hardness of the non-quenched zone should not exceed 35HRC [12]. However, there exist few innovative designs for the structure of the key cutting components, and studies concerning the relationship between the structure of key components and the performance of castor cutting systems are limited. Therefore, further study of cutting systems for castor harvester picking devices is required.

With the improvement of computer processing technology, the use of numerical analysis is becoming increasingly common in agricultural engineering. Considering accuracy and economical calculation, the finite element method is one of the best ways to study the factors affecting castor harvesting. Numerical simulation technology was used to simulate the crop stalk cutting process. This approach could provide a research tool and theoretical basis for the design of a castor harvester and reduce the time and cost involved in machinery research and development. In recent years, LS-DYNA simulation software has been widely used to study the results of material deformation or failure in the agricultural field. Huang et al. [13] used ANSYS/LS-DYNA to conduct numerical calculations and simulations on a finite element model composed of different cutting angles and speeds in the sugarcane cutting process. Meng et al. [14] used ANSYS/LS-DYNA to simulate a circular saw blade model under different conditions for the cutting of mulberry branches and determined the optimal parameters for the circular saw blade. Based on a Box–Behnken design experiment, Xie et al. [15] established models for the sugarcane cutting process which simulated the cutting resistance and stress distribution of blades and sugarcane under different factors. These models were used to determine the optimization parameters according to sugarcane cutting quality and the average maximum cutting power consumption. Cao et al. [16] used LS-DYNA software to simulate the picking process of a carp-clip safflower picking device and revealed the relationship between the different structural and working parameters of the picking device and the safflower movement type. Souza et al. [17] carried out finite element analysis of the interaction between harvester rods and coffee branches using ANSYS/LS-DYNA software and tested the samples with plagiotropic coffee branches. Ibrahmi et al. [18] studied the dynamic impact of the apple using the finite element method and carried out the apple collision tests.

The FEM method involves the encryption of the mesh of the contact part, focusing on material failure and damage in the cutting process. This simulation method is generally based on element deletion technology, which ignores conservation and, to a certain extent, affects the accuracy of the cutting force analysis. The SPH algorithm does not have the mesh distortion and element failure problems and, in comparison with other methods, has very significant advantages in terms of failure types [19–21]. However, because of the algorithm differences, the computational efficiency of the SPH method is low and boundary conditions are difficult to solve. For this reason, some scholars have proposed the SPH–FEM coupling method [22–24]. The FEM algorithm is used to solve the low-speed deformation region in the model analysis, and the SPH algorithm is used to solve the high deformation, high speed, and difficult FEM calculation region. The advantages of the two

algorithms, such as a low speed, small deformation area, accurate Lagrange solution, fast solution speed and a large deformation area to avoid the increase in computational load caused by mesh distortion, are fully used to solve the coexisting coupling problems of large deformation, impact, small deformation, etc.

Based on the above summary, the cutting system is the most important part of castor harvester picking devices and affects the performance and power consumption of castor harvesters. Focusing on wave-type disc cutters of the designed cutting system, the cutting process was analyzed and the parameters optimized. The objective of this paper was to perform a simulation of the castor stalk-cutting process using the coupled SPH–FEM numerical calculation method based on stalk physical characteristics [25–28] and then to optimize the structural and operating parameters of the disc cutter using the orthogonal rotation combination test. Finally, the numerical computer simulation results were verified via experimental tests.

2. Materials and Methods

2.1. Machine Structure and Working Principles

2.1.1. Main Structure

The castor harvester picking device was designed based on a previous study, as shown in Figure 1. The device is attached to a rice or corn combine, which has low requirements for line alignment, has good agronomic planting adaptability and does not miss plants when harvesting.

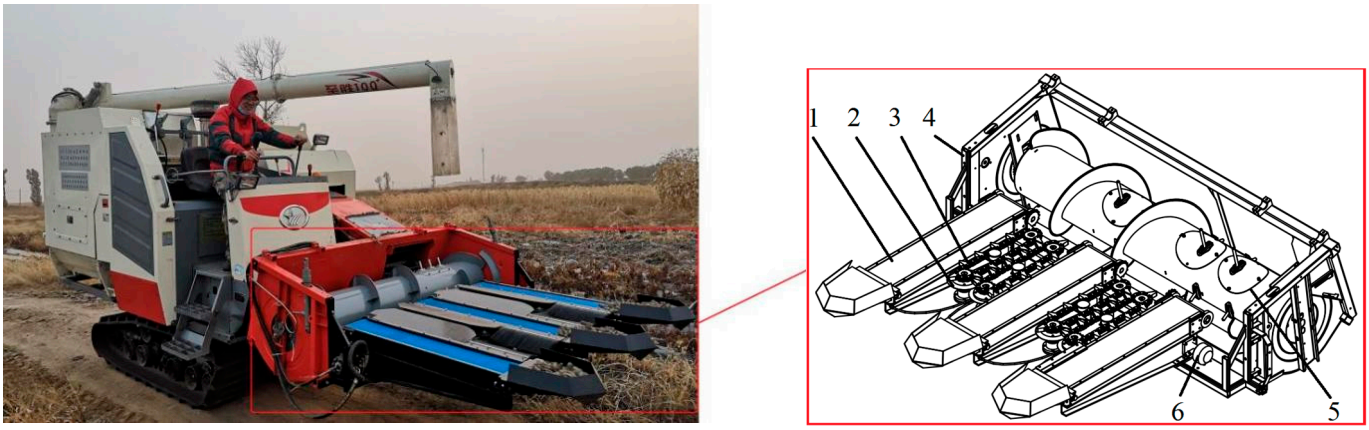


Figure 1. Castor harvester picking device. 1. Capsule recycling mechanism; 2. double-disc cutting system; 3. dial teeth chain; 4. frame; 5. horizontal auger; 6. transmission system.

The castor harvester picking device is mainly composed of the frame, the capsule recycling mechanism, the double-disc cutting system, the dial teeth chain, and the transmission system. The main structural dimensions are shown in Table 1. The double-disc cutting system is primarily composed of the disc cutter, dial teeth chain, etc. The main component of the capsule recycling mechanism is the conveyor belt. For picking two rows, the picking device is configured with four disc cutters, three conveyor belts, and four closed dial teeth chains.

Table 1. Main technical parameters of the castor harvester picking device.

Item	Values	Item	Values
Boundary dimension/ (mm × mm × mm)	2360 × 2262 × 567	Working width/(mm)	1500
Working speed/(m·s^{-1})	0~1.58	Rows picked/row	2

The structure of the disc cutter in the cutting system of the castor harvester picking device is an important element that affects harvesting quality and efficiency [29–31]. Ac-

cording to previous test results [32], the structural parameters of the disc cutter are as shown in Figure 2.

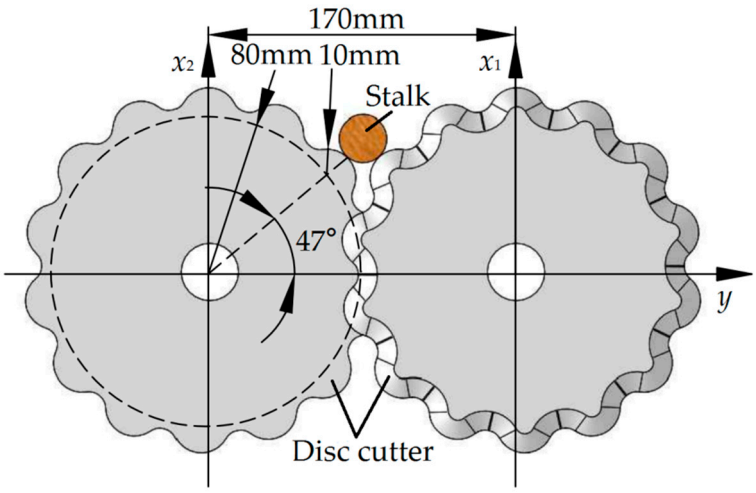


Figure 2. Double-disc cutting system consisting of wave-type disc cutters.

2.1.2. Working Principles

During castor harvesting operations, power from the hydraulic motor is transmitted to the dial teeth chain. The disc cutter is coaxial with the driven sprocket of the dial teeth chain. The motion of the adjacent dial teeth chain causes the two disc cutters in the cutting system to rotate in opposite directions and cut the castor stalk. Then, the cut castor plants are pushed back to the horizontal auger by the dial teeth chain. At the same time, the shocking or striking of the device causes the castor capsules to fall toward the capsule recycling mechanism and then to be transported to the horizontal auger by the conveyor. Finally, the plants (including the fallen capsules) are transported to the cleaning device of the harvester, completing the castor harvesting operation.

It can be seen that the double-disc cutting system cuts the whole castor plant during castor harvesting, which has an important effect on the performance of castor harvester.

2.2. Mechanical Analysis

By analyzing the force in the cutting process, clarifying the interaction between the cutter disc and the castor stalk, and studying the stalk-cutting mechanism, the main factors affecting the cutting force were determined. The castor stalk-cutting process was divided into contact and cutting stages according to the different positions and states in the study.

2.2.1. Contact Stage

The maximum stress at the contact stage occurs at the moment when the stalk changes from a static state, gains kinetic energy and withstands the impact of the disc cutter. The contact and collision process between castor stalk and disc cutter was analyzed. The force and velocity analysis of the stalk are shown in Figure 3. The disc is in contact with the stalk at a relative velocity V_z. When the velocity of the stalk increases to the same level as that of the disc cutter, their relative velocity is zero. The relative displacement δ_z between the stalk and the disc cutter does not decrease. In this case, the maximum contact force is P_{max}.

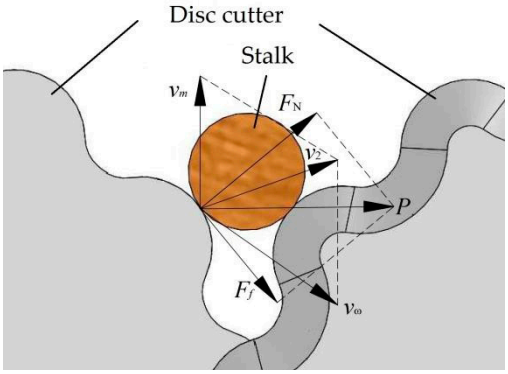


Figure 3. Schematic of stalk contact force and velocity.

According to inelastic collision theory, the relative displacement δ_z at a given moment is as follows:

$$a = \left(\frac{3PR}{4E^*}\right)^{\frac{1}{3}} \tag{1}$$

$$\delta_z = \frac{a^2}{R} = \left(\frac{9P^2}{16RE^{*2}}\right)^{\frac{1}{3}} \tag{2}$$

$$\frac{1}{E^*} = \frac{(1-v_1^2)}{E_1} + \frac{(1-v_2^2)}{E_2} \tag{3}$$

$$\frac{1}{R} = \frac{1}{R_1} + \frac{1}{R_2} \tag{4}$$

$$\frac{1}{m} = \frac{1}{m_1} + \frac{1}{m_2} \tag{5}$$

where a is the effective dimension of contact segment m; P is the loading force, N; R is the relative radius of curvature, m; E^* is the elasticity modulus, MPa; δ_z is the displacement of contact point, m; v_1 is the contact velocity of the stalk, m/s; E_1 is the elasticity modulus of the stalk, MPa; v_2 is the contact velocity of the disc cutter, m/s; E_2 is the elasticity modulus of the disc cutter, MPa; R_1 is the effective radius of the stalk, m; R_2 is the effective radius of the disc cutter, m; m is the equivalent mass, kg; m_1 is the mass of the stalk, kg; and m_2 is the mass of the disc cutter, kg.

During the collision process, because of elastic deformation, the centers of the stalk and disc cutter approach each other by a displacement δ_z, and their relative velocity is as follows:

$$v_2 - v_1 = \frac{d\delta_z}{dt} \tag{6}$$

At any instant, the interaction force is as follows:

$$P(t) = m_1\frac{dv_1}{dt} = -m_2\frac{dv_2}{dt} \tag{7}$$

This can be obtained using the following Equations (6) and (7):

$$-\frac{m_1+m_2}{m_1m_2}P = \frac{d(v_2-v_1)}{dt} = \frac{d^2\delta_z}{dt^2} \tag{8}$$

According to Equation (2), the following can be obtained:

$$P = \frac{4}{3}R^{1/2}E^*\delta_z^{3/2} = K\delta_z^{3/2} \tag{9}$$

Substituting Equations (5), (8) and (9), the following can be obtained:

$$m\frac{d\delta_z}{dt} = -K\delta_z^{3/2} \tag{10}$$

The following can be obtained by integrating δ_z:

$$\frac{1}{2}\left[V_z^2 - \left(\frac{d\delta_z}{dt}\right)^2\right] = \frac{2K}{5m}\delta_z^{5/2} \tag{11}$$

$$V_z = (v_2 - v_1)_{t=0} \tag{12}$$

where V_Z is the velocity of the stalk and the disc cutter approaching each other, m/s.

At the maximum compression displacement, $d\delta_z/dt = 0$, using Equation (11) we can obtain the following:

$$\delta_z^* = \left(\frac{5mV_Z^2}{4K}\right)^{2/5} = \left(\frac{15mV_Z^2}{16R^{1/2}E^*}\right)^{2/5} \tag{13}$$

According to the Von Mises criterion, at the time of initial yield, the relationship between maximum contact pressure P_{max} and loading force is as follows:

$$P_{\max} = \left(\frac{6P \cdot E^{*2}}{\pi^3 \cdot R^2}\right)^{\frac{1}{3}} \tag{14}$$

By substituting Equations (9), (13), and (14), the maximum force in the contact process is obtained as follows:

$$P_{max} = \frac{3}{2\pi}\left(\frac{4E^*}{3R^{\frac{3}{4}}}\right)^{\frac{4}{5}} \cdot \left(\frac{5}{4}mV_z^2\right)^{\frac{1}{5}} \tag{15}$$

During the contact process, when the maximum contact stress P_{max} exceeds the elastic limit of the stalk, the stalk undergoes plastic deformation and enters the cutting stage. According to Equation (15), the maximum contact force of the disc cutter is positively correlated with the contact relative velocity of the stalk and the equivalent mass of the stalk and disc cutter, and negatively correlated with the equivalent radius of curvature.

2.2.2. Cutting Stage

When the castor stalks are cut with the disc cutter, the edge and surface of the disc cutter are the key parts that cut the stalk and resist the cutting force. Therefore, this study analyzed the mechanical model of cutting resistance in terms of differentials. As shown in Figure 4, the cutting resistance of the disc cutter at the moment of cutting mainly includes the reaction force F_0 exerted by the stalk against the motion of the disc cutter at the cutting edge, the extrusion force F_{1x}, F_{1y} and friction T_2 of the stalk pressed on the external edge surface, and the extrusion force F and friction T_1 of the stalk pressed on the internal edge surface.

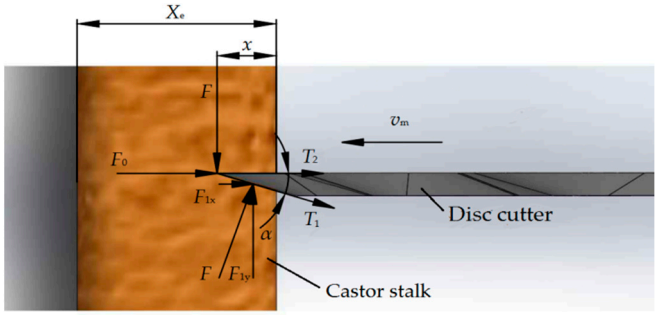


Figure 4. Cutting force of the stalk.

The stalk is analyzed as a whole unit with certain physical characteristics. The external edge surface is divided using a differential method. The extrusion force dF_{1x} on the external edge differential element plane in the X direction (that is the direction v_m of the disc cutter motion velocity) is obtained as follows:

$$dF_{1x} = \sigma l dy = \sigma l dx \cdot \tan \alpha \tag{16}$$

where F_{1x} is the extrusion force on the external edge surface of the disc cutter in the X direction N; σ is the crushing stress in the X direction, MPa; l is the cutting width, m; and α is the edge angle, °.

The stress and strain of the stalk during the cutting process was determined using Hooke's law, and the stress–strain relationship of the stalk cutting is as follows:

$$\varepsilon = \frac{X_e}{x} = \frac{\sigma}{E_x} \tag{17}$$

where ε is the shear strain; X_e is the total stalk thickness, m; x is the stalk thickness when pressed by the cutter disc, m; and E_x is the elastic modulus of the stalk in the X direction, MPa.

Next, we substitute Equation (17) into Equation (16) and integrate dF_{1x}. The extrusion force F_{1x} is as follows:

$$F_{1x} = \int_0^x \sigma l \tan \alpha dx = \int_0^x \frac{x}{X_e} E_x l \tan \alpha dx = \frac{x^2 l}{2X_e} E_x l \tan \alpha \tag{18}$$

The extrusion force on the external edge differential element plane in Y direction dF_{1y} is as follows:

$$dF_{1y} = \varepsilon_y E_y l dx = \varepsilon_x \mu E_y l dx \tag{19}$$

where F_{1y} is the extrusion force on the external edge surface of disc cutter in the Y direction, N; ε_y is the cutting strain of the castor stalk in the Y direction; and E_y is the elastic modulus of the stalk in the Y direction, MPa.

The extrusion force F_{1y} of the external edge surface in the Y direction is as follows:

$$F_{1y} = \int_0^x \varepsilon_x \mu E_y l dx = \int_0^x \frac{x}{X_e} \mu E_y l dx = \frac{x^2 l}{2X_e} \mu E_y l \tag{20}$$

The friction force T_1 on the external edge is as follows:

$$T_1 = \mu \left(F_{1x} \cdot \sin \alpha + F_{1y} \cdot \cos \alpha \right) = \frac{x^2 l}{2X_e \cos \varepsilon} \left(E_x \sin^2 \alpha + \mu_\omega E_y \cos^2 \alpha \right) \tag{21}$$

where T_1 is the friction force on the external edge, N; and μ is the coefficient of dynamic friction between the blade surface and stalk.

$$F_0 = \delta l \sigma_c \tag{22}$$

Here, F_0 is the acting force of the stalk on the disc cutter, N; δ is the disc cutter thickness, m; and σ_c is the yield strength, MPa.

$$T_2 = \mu_i F \tag{23}$$

Here, T_2 is the friction force on the internal edge, N; μ_i is the coefficient of stalk internal friction; and F is the pressure of the disc cutter against the stalk, N.

At the cutting moment, the total cutting resistance of the disc cutter is as follows:

$$\begin{cases} F_X = F_0 + F_{1x} + T_1 + T_2 \cdot \cos \alpha \\ F_Y = F + T_2 \cdot \sin \alpha \end{cases} \tag{24}$$

where F_X is the cutting force in the X direction, N; and F_Y is the cutting force in the Y direction, N.

Based on the above theoretical analysis, it can be seen that the cutting force of the disc cutter is closely linked to the physical properties of the stalk and the structural and technological parameters of the disc cutter. In order to reduce power consumption in the process of castor harvesting, the cutting resistance mechanical model must be considered when optimizing the design of the cutting device. Therefore, to reduce the cutting resistance, influencing factors, such as the disc cutter thickness and edge angle, were selected for further study.

2.3. Cutting Process Simulation Model

In this paper, the explicit dynamics software LS-DYNA was used to establish a simulation model of castor stalk cutting, and the cutting process was simulated using different parameters. This method provided a theoretical basis for subsequent field tests.

2.3.1. Simulation Model

For reasonable and effective simulation and calculation, the disc cutter model was simplified to remove the parts unrelated to the cutting process. SolidWorks software was used to model the disc cutter which was then imported into the simulation software. The material attribute of the disc cutter was $45^{\#}$ steel [33] with a Poisson's ratio of 0.31, shear modulus of 7.9×10^{10} Pa and density of 7850 kg/m^3.

An Israel Kaifeng 5 castor stalk with a diameter of 22 mm was modeled. To reduce the simulation time without significantly affecting the simulation effect, a 150 mm section was modeled to represent the stalk. The physical parameters of the castor stalk with a water content of 20% [34–36] are displayed in Table 2.

Table 2. Physical characteristics of a castor stalk.

Stalk	Density (kg·m^{-3})	Elasticity Modulus (MPa)	Poisson's Ratio	Shear Modulus (MPa)	Yield Strength (MPa)
Value	1080	13.3	0.252	4.37	110

The stalk model used in this study was divided into three parts, as shown in Figure 5. During the cutting process, part of the finite element mesh was not in contact with the disc cutter. The SPH particle was defined as the slave node, and the finite element mesh at the contact interface with the SPH particle was the main surface. The contact algorithm was * CONTACT-AUTOMATIC-NODES-TO-SURFACE.

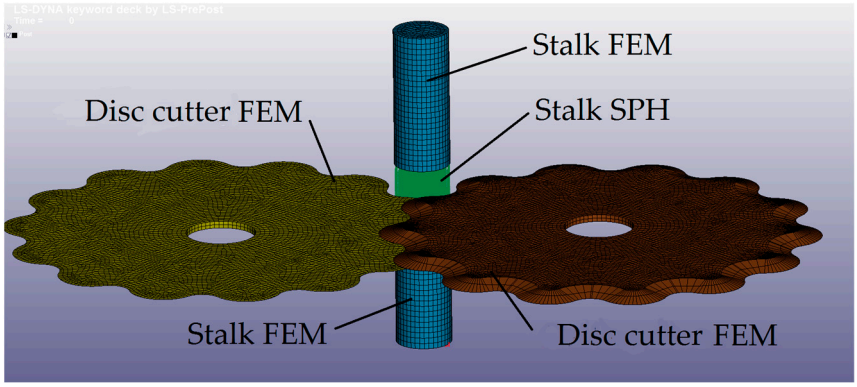


Figure 5. Simulation model using LS-DYNA software.

2.3.2. Contact Erosion Definition and Loading

Setting the coefficient of static friction F_S = 0.3 and the coefficient of kinetic friction F_D = 0.2 [37], the node-set on the two disc cutting model applied the moving speed of the *X*-axis and the rotation speed in the opposite rotation of the *Z*-axis. The corresponding K file was generated by setting the simulation data using LS-PrePost software and then submitting them to the LS-DYNA software for computation.

2.4. Simulation Test Design

2.4.1. Test Evaluation Index

To ensure the durability of the disc cutter, cutting resistance has a decisive influence in optimizing the design of the disc cutter structure. Precompression elastic deformation causes the cutting force to rise to its peak. Excessive instantaneous cutting force makes it easy to damage the cutter teeth in the cutting process. Therefore, the maximum cutting force is an index to be investigated in this study. During the test, a torque sensor (Beijing Xinyuhang Measurement and CT Co., Ltd., model: JN338, measuring time range: 20–2000 ms) was used to measure the torque of the unilateral disc cutter and the maximum cutting force was calculated according to the peak of the torque curve.

According to Equation (25), the maximum cutting force F_{max} calculation formula is as follows:

$$F_{max} = \frac{T}{R} \tag{25}$$

where F_{max} is the maximum cutting force, N; R is the radius of disc cutter, m; and T is the torque, N·m.

2.4.2. Test Factors and Levels

According to the above analysis, the factors affecting the maximum cutting force include the disc cutter thickness, edge angle, disc cutter rotation speed, and feeding speed. A quadratic rotation orthogonal combination test was used. The test factors and levels are shown in Table 3.

Table 3. Test factors and levels.

level	Disc Cutter Thickness (mm)	Disc Cutter Rotation Speed (r·min^{-1})	Feeding Speed (m·s^{-1})	Edge Angle (°)
−2	2	400	0.4	15
−1	3	550	0.6	20
0	4	700	0.8	25
1	5	850	1.0	30
2	6	1000	1.2	35

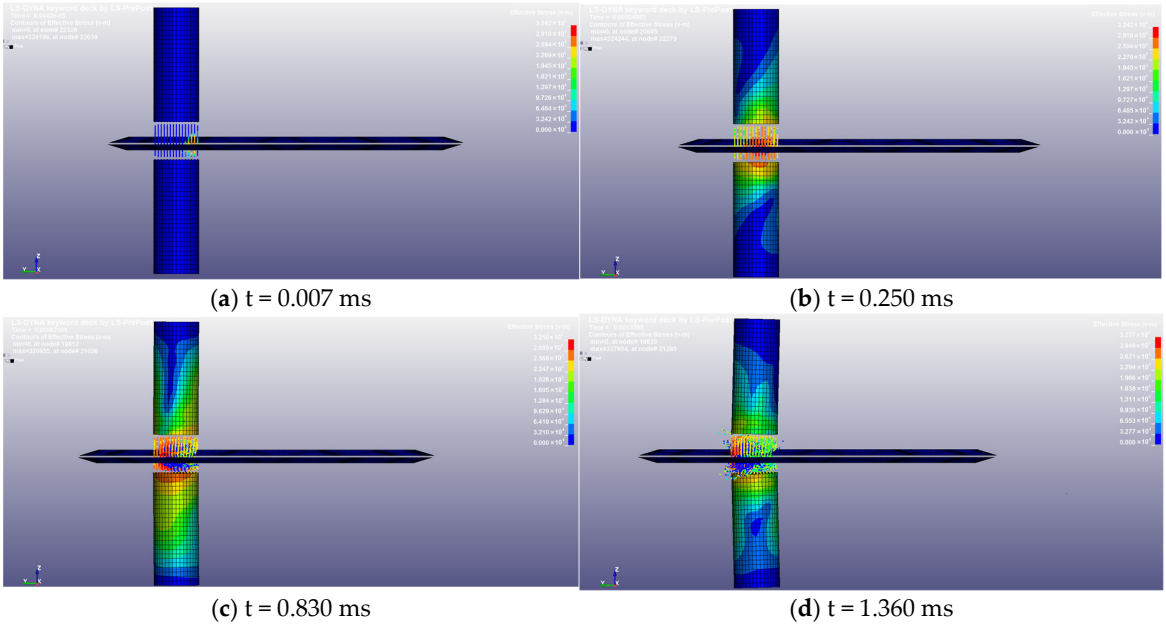
3. Results Analysis and Optimization

3.1. Simulation Results

Castor stalk cutting is a process in which the disc cutter repeatedly enters the stalk, cuts it, and releases its elastic and plastic stress. It is primarily divided into three stages, namely the contact stage, cutting stage, and cracking stage. The castor stalk-cutting process is shown in Figure 6.

As shown in Figure 6a, at the contact stage, the stalk was clamped with the bilateral disc cutter, resulting in some compressive shear failure units at the edge. At this time, the stalk mainly produced elastic strain and remained relatively intact. Because of the fast rotation speed of the disc cutter, there were two wavy arcs on the disc cutter that cut the stalk within the stalk diameter. The cutting stage was divided into the first cutting stage and second cutting stage according to the cutting conditions of the different waved blades. At the first cutting stage, as shown in Figure 6b, the wave-type disc cutter cut into the castor stalk and generated an extremely high-stress area on the surface of the stalk. The stalk underwent elastic–plastic deformation so that it directly formed symmetric deformation

and failure in the axial direction. At this time, the stress was mainly distributed along the middle and side direction of the cutting part. In addition, the stalk that had been cut was also subjected to friction stress on the disc cutter surfaces, and the maximum stress occurred at this cutting stage. In the second cutting stage (Figure 6c), the cutting length and invasion depth increased. The anterior part of the stalk axial direction was completely cut off, forming a wedge-shaped failure zone. This zone was mainly composed of compression failure elements, and the elastic–plastic strain energy in this zone decreased. The sheared part of the stalk produced extremely small cuttings. In addition to the large stress caused by the cutting edge on the stalk, the friction force caused by the disc cutter was small. Thus, the stress value was lower than that produced at the first cutting stage.



(**a**) t = 0.007 ms (**b**) t = 0.250 ms

(**c**) t = 0.830 ms (**d**) t = 1.360 ms

Figure 6. Postprocessing of the simulation. (**a**) Effective stress at 0.007 ms; (**b**) effective stress at 0.250 ms; (**c**) effective stress at 0.830 ms; and (**d**) effective stress at 1.360 ms.

As displayed in Figure 6d, the failure zone of the disc cutter was further expanded and the cuttings were able to crack outward. Under the action of the high-speed disc cutter, the stalk bent significantly and broke. Because most of the elastic and plastic stress of the stalk had been released, the overall stress value of the stalk was small.

3.2. Results and Analysis

Quadratic regression analysis and multiple regression fitting were performed on the test results using Design-Expert software. A total of 30 treatments were conducted, as shown in Table 4.

The regression and factor variance analyses were carried out on the test data using Design-Expert, and the factors with significant influence were screened out, as shown in Table 5.

It can be seen from Table 5 that the regression model was significant ($p < 0.01$) and that the lack of fit was extremely insignificant ($p > 0.05$). The results indicated that the model terms and the factors on the maximum cutting force were extremely significant.

Table 4. Test schemes and results.

Serial Number	Disc Cutter Thickness (mm)	Disc Cutter Rotation Speed (r·min^{-1})	Feeding Speed (m·s^{-1})	Edge Angle (°)	Maximum Cutting Force Y_1 (N)
1	0	0	0	0	134.7
2	−1	1	−1	1	86.3
3	1	−1	−1	1	143.9
4	0	0	0	0	128.7
5	1	1	1	−1	71.2
6	−1	1	1	1	56.4
7	0	0	2	0	74.4
8	0	0	0	−2	144.2
9	0	0	0	0	124.7
10	1	−1	−1	−1	146.3
11	−2	0	0	0	133.8
12	−1	−1	−1	−1	198.1
13	2	0	0	0	107.2
14	0	−2	0	0	181.6
15	0	0	0	0	113.7
16	1	−1	1	−1	100.1
17	0	0	0	0	124.7
18	−1	−1	1	1	120.6
19	−1	−1	−1	1	126.3
20	0	0	0	2	88.6
21	1	1	1	1	73.9
22	1	1	−1	1	97.8
23	1	−1	1	1	111.2
24	1	1	−1	−1	110.8
25	−1	−1	1	−1	168.6
26	−1	1	1	−1	76.2
27	0	2	0	0	97.3
28	−1	1	−1	−1	146.7
29	0	0	0	0	136.7
30	0	0	−2	0	149.3

Table 5. Variance analysis.

Serials	Maximum Cutting Force Y_1 (%)			
	Sum of Squares	Degree of Freedom	*F* Value	*p* Value
Model	31,473.42	14	23	<0.0001
A	1308.33	1	13.38	0.0023
B	13,272.81	1	135.78	<0.0001
C	7625.54	1	78.01	<0.0001
D	4076.83	1	41.71	<0.0001
AB	627.5	1	6.42	0.0229
AC	2.89	1	0.03	0.8658
AD	2460.16	1	25.17	0.0002
BC	155	1	1.59	0.2272
BD	26.52	1	0.27	0.61
CD	547.56	1	5.6	0.0318
A^2	232	1	2.37	0.1442
B^2	91.77	1	0.94	0.3479
C^2	705.28	1	7.22	0.0169
D^2	424.35	1	4.34	0.0547
Residual	1466.25	15		
Lack of fit	1122.75	10	1.63	0.3062
Pure error	343.5	5		
Total	32,939.67	29		

3.3. Regression Equations

We eliminated the nonsignificant items and ensured that all factors reached the significant or extremely significant level. The regression equation of the maximum cutting force can be expressed as follows:

$$Y_1 = +127.2 - 7.38x_1 - 23.52x_2 - 17.82x_3 - 13.03x_4 + 6.26x_1x_2 + 12.40x_1x_4 + 5.85x_3x_4 - 5.07{x_3}^2 \quad (26)$$

According to the variance table, the primary terms x_1, x_2, x_3, and x_4, interaction term x_1x_4, and quadratic terms ${x_3}^2$ have a significant impact on the maximum cutting force ($p < 0.01$). The interaction terms x_1x_2 and x_3x_4 have significant effects on the maximum cutting force ($0.01 < p < 0.05$). The weights of the factors affecting the maximum cutting force are as follows: disc cutter rotation speed x_2 > feeding speed x_3 > edge angle x_4 > disc cutter thickness x_1.

3.4. Analysis of the Response Surface

In order to intuitively analyze the relationship between test factors and indexes, the response surface diagram was obtained using Design-Expert software together with the multifactor test data. The response surface is shown in Figure 7.

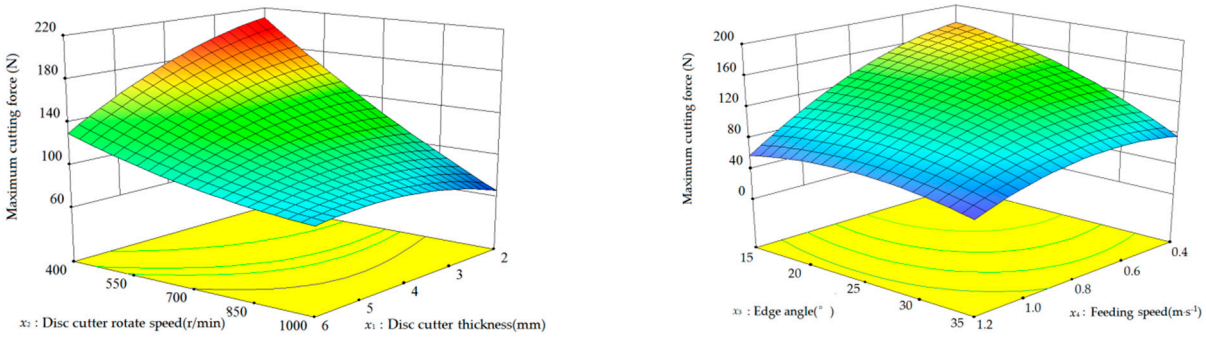


Figure 7. Response surface of the maximum cutting force. (**a**) Interaction factors of disc cutter rotation speed and thickness; And (**b**) interaction factors of edge angle and feeding speed.

Figure 7a shows the interaction between disc cutter thickness and disc cutter rotation speed on the maximum cutting force when the feeding speed and edge angle are at an intermediate level. It can be concluded from Figure 7a that when the disc cutter rotation speed is lower, the maximum cutting force increases notably with the increase in the disc cutter thickness. However, when the disc cutter rotation speed is higher, this trend is relatively gentle. As the thickness of the disc cutter increases, the fiber undergoes elastic–plastic recovery and squeezes the disc cutter, which leads to greater cutting surface resistance and an increase in the maximum cutting force of the disc cutter. When the disc cutter rotation speed is low, the castor stalk only partially produces sufficient elastic–plastic deformation. Therefore, the friction force of the disc cutter caused by the elastic–plastic deformation is larger, and the maximum cutting force significantly increased. When the disc cutter rotation speed is high, the stalk is cut at one time and there is less local elastic–plastic deformation. The failure process tends to be a one-time fracture, and the maximum cutting force increases slowly.

According to the correlation regression equation and the density of contour distribution in the response surface, the maximum cutting force is influenced by the interaction between the edge angle and the feeding speed, as shown in Figure 7b. When the edge angle is small, the maximum cutting force decreases significantly with increased feeding speed. When the edge angle is large, the maximum cutting force increases slowly and then flattens out as the feeding speed increases. The main reason for this is that the smaller cutting angle usually results in higher local stress, which makes it easier to break the stalk fiber, and the maximum cutting force is, therefore, smaller. The sliding-cutting angle is negatively correlated with the cutting resistance. With a small edge angle, a faster feeding speed causes a notable increase in the sliding-cutting angle and the maximum cutting force decreases. When the edge angle is larger, the physical structure resistance of the cutting

edge is larger, and the increase in the sliding-cutting angle is insignificant, resulting in a nonsignificant increase in the maximum cutting force.

3.5. Parameter Optimization

In order to obtain the best cutting parameters for a wave-type disc cutter, the optimization module of the Design-Expert software was used to optimize and solve the regression model. Its constraint conditions were as follows:

$$\begin{cases} s.t. \begin{cases} 2 \le A \le 6 \\ 400 \le B \le 1000 \\ 0.4 \le C \le 1.2 \\ 15 \le D \le 35 \end{cases} \\ \min Y_1(A, B, C, D) \end{cases} \quad (27)$$

The multiobjective optimization solution was calculated as follows: a disc cutter thickness of 2.71–3.15 mm, a disc cutter rotation speed of 844.2–942.1 r/min, a feeding speed of 0.89–1.01 m/s, and an edge angle of 29.2–33.9°, where the maximum cutting force is less than 50 N.

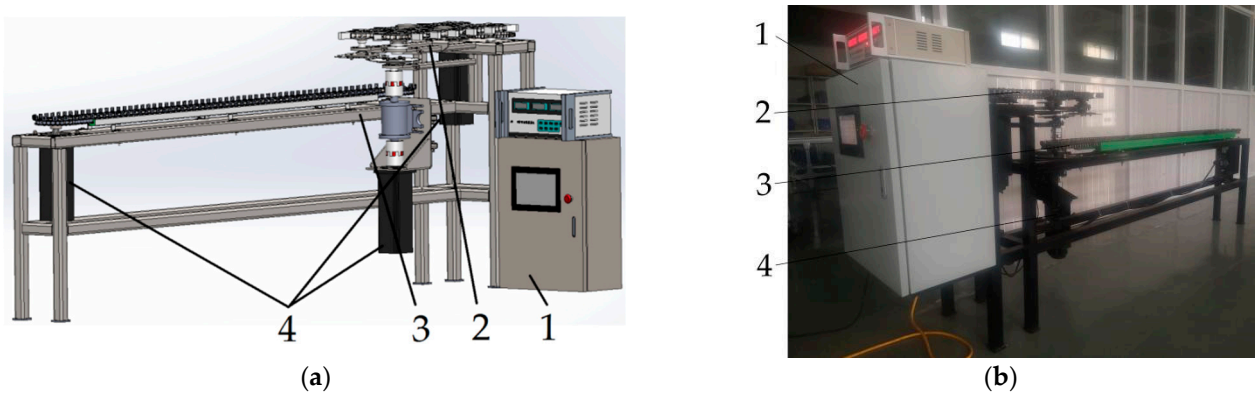
4. Verification Test Results

4.1. Test Materials and Devices

The verification test bench was built in September 2022. The main instruments used were as follows: a sensor (Beijing Xinyuhang Measurement and CT Co., Ltd., model JN338-A); a torque speed measuring instrument (Beijing Xinyuhang Measurement and CT Co., Ltd., model JN338); a transport motor (Beijing Times Superior Electrical Technology Co., Ltd., model SD110AEA12020-SH3, rated power 1.2 kW, rated speed 2000 rad/min, rated moment 6 N/m); a cutting motor (Beijing Times Superior Electrical Technology Co., Ltd., model SD110AEA12020-SH3, rated power 1.5 kW, rated speed 1500 rad/min, rated moment 10 N/m); and a driver (Beijing Times Superior Electrical Technology Co., Ltd., model SD300-30AL-GBN).

As shown in Figure 8, the verification test was carried out on the test bench. A 10A single-sided double-hole bending plate chain was selected as the stalk sample conveyor chain. The disc cutter on one side was coaxial with the cutting motor and torque sensor through the detachable flange. The disc cutter on the other side was coaxial with the dial teeth chain and the cutting motor. The torque measuring instrument was connected to the sensor and communicated with the computer in real-time through the RS232 serial port. During the test, the drivers were firstly used to drive the cutting motors to the designed rotation speed, and then the other driver was used to drive the feed motor to clamp and advance the samples at the set speed until the cutting process was completed. With this test device, the disc cutter could be changed and the feeding and cutting rotation speeds could be adjusted and measured. The maximum cutting torque of the disc cutter was obtained by using the torque measuring instrument to study the maximum force in the cutting process.

The castor cultivar was Israel Kaifeng No.5. After the cutting test, the cut part of the stalk was used as for the determination of the physical properties. The average diameter of the castor stalk at 150 mm from the ground was 21.6 mm.



(**a**) (**b**)

Figure 8. Verification test device. (**a**) Schematic diagram. (**b**) Cutting test bench—1. measurement and control system; 2. cutting system; 3. feeding device; and 4. dynamical system.

4.2. Test Results

To test the optimal combination of parameters for the disc cutter, the operating parameters were set as follows: the disc cutter thickness at 3 mm, the disc cutter rotation speed at 942 r/min, the feeding speed at 1.0 m/s, and the edge angle at 30°. In these conditions, the predicted value of the maximum cutting force was 42.64 N according to Equation (26). The verification test was repeated five times, and the results are recorded in Table 6.

Table 6. Bench test results.

Item	Optimization Value	Verification Test				
		1	2	3	4	5
Maximum cutting force (N)	42.64	43.5	45.8	46.1	41.5	46.2

Through experimental verification, the experimental data were compared with the numerical simulation data. The analysis showed that the test results were generally consistent with the simulation results and that the error was less than 10%. The experimental data were slightly higher than the simulation data. The results indicated that the simulation model was effective and reasonable and could provide technical support for the design of castor harvesters.

5. Conclusions

In order to reduce the cutting resistance of wave-type disc cutters in the picking devices of castor harvesters, this study used the SPH–FEM coupling algorithm and LS-DYNA software to simulate the dynamic process of cutting castor. Based on the orthogonal rotation combination test, the effects of disc cutter thickness, disc cutter rotation speed, feeding speed, and disc cutter edge angle on the maximum cutting force were simulated. The simulation results were optimized using the response surface method, and the optimal combination of parameters was verified using experimental tests. The conclusions were as follows:

(1) Simulation tests showed that the disc cutter rotation speed, feeding speed, disc cutter thickness, and edge angle had a highly significant influence on the maximum cutting force. The influence of each factor on the maximum cutting force was in the order of disc cutter rotation speed > feeding speed > edge angle > disc cutter thickness. The following optimal parameters were obtained: disc cutter thickness of 2.71–3.15 mm, disc cutter rotation speed of 844.2–942.1 r·min^{-1}, feeding speed of 0.89–1.01 m·s^{-1}, and edge angle of 29.2–33.9°, where the maximum cutting force was less than 50 N;

(2) The operating parameters were set as follows: disc cutter thickness at 3 mm, disc cutter rotation speed at 942 r/min, feeding speed at 1.0 m/s, and edge angle at 30°,

with a predicted maximum cutting force of 42.64 N. The verification test indicated that the maximum cutting force obtained by the SPH–FEM coupling simulation method was generally consistent with the castor-cutting bench test using the optimized combination of parameters and that there was no significant difference in the data obtained using the two methods. The simulation method can, therefore, be used to study castor harvester disc cutters and provides an effective method for further parameter optimization of castor disc cutters.

Author Contributions: Conceptualization, F.K., D.W. and L.S.; methodology, Q.X., Y.S. and C.C.; software, Q.X., H.H. and T.W.; validation, D.W., L.S. and Y.S.; writing—original draft preparation, F.K., D.W. and T.W.; writing—review and editing, F.K., D.W. and H.H. All authors have read and agreed to the published version of the manuscript.

Funding: This research was funded by the Agricultural Science and Technology Innovation Program of Chinese Academy of Agricultural Sciences (CAAS-ASTIP-31-NIAM-05) and supported by National Natural Science Foundation of China (52205261).

Institutional Review Board Statement: Not applicable.

Informed Consent Statement: Not applicable.

Data Availability Statement: Not applicable.

Acknowledgments: We greatly appreciate the careful and precise reviews provided by the anonymous reviewers and editors.

Conflicts of Interest: The authors declare no conflict of interest.

References

1. Alexopoulou, E.; Papatheohari, Y.; Zanetti, F.; Tsiotas, K.; Papamichael, I.; Christou, M.; Namatov, I.; Monti, A. Comparative studies on several castor (*Ricinus communis* L.) hybrids: Growth, yields, seed oil and biomass characterization. *Ind. Crops Prod.* **2015**, *75*, 8–13. [CrossRef]
2. Pari, L.; Suardi, A.; Stefanoni, W.; Latterini, F.; Palmieri, N. Environmental and Economic Assessment of Castor Oil Supply Chain:A Case Study. *Sustainability* **2020**, *12*, 6339. [CrossRef]
3. Suurbaar, J.; Mosobil, R.; Donkor, A.M. Antibacterial and antifungal activities and phytochemical profle of leaf extract from diferent extractants of Ricinus communis against selected pathogens. *BMC Res. Notes* **2017**, *10*, 660. [CrossRef]
4. Severino, L.S.; Auld, D.L. A framework for the study of the growth and development of castor plant. *Ind. Crops Prod.* **2013**, *46*, 25–38. [CrossRef]
5. Baldanzi, M.; Fambrini, M.; Pugliesi, C. Redesign of the castorbean plant body plan for optimal combine harvesting. *Ann. Appl. Biol.* **2003**, *142*, 299–306. [CrossRef]
6. Wu, C.F.; Chen, W.C.; Sheng, C.T. Study on the harvester development of ricinus communis. *J. Agric. Fore.* **2013**, *62*, 33–44.
7. Liu, L.; Wu, T.; Kong, F.T.; Sun, Y.F.; Chen, C.L.; Xie, Q.; Shi, L. Optimized design and experiment of the picking mechanism for brush-roller castor harvesters. *Trans. Chin. Soc. Agric. Eng.* **2021**, *37*, 19–29.
8. Stefanoni, W.; Latterini, F.; Malkogiannidis, V.; Salpiggidis, V.; Alexopoulou, E.; Pari, L. Mechanical Harvesting of Castor Bean (Ricinus communis L.)with a Combine Harvester Equipped with Two Different Headers: A Comparison of Working Performance. *Energies* **2022**, *15*, 2999. [CrossRef]
9. Rostek, T.; Homberg, W. Locally graded steel materials for self-sharpening cutting blades. *Procedia Eng.* **2017**, *207*, 2185–2190. [CrossRef]
10. Song, Y.P.; Wu, K.; Wang, W. Fabrication of self-sharpening blades via vacuum-rolling composite technology and its interfacial material microstruature and properties. *Trans. Chin. Soc. Agric. Eng.* **2020**, *51* (Suppl. 2), 586–592.
11. Momin, M.A.; Wempe, P.A.; Grift, T.E. Effects of four base cutter blade designs on sugarcane stem cut quality. *Trans. ASABE* **2017**, *60*, 1551–1560. [CrossRef]
12. Wu, K.; Song, Y.P. Research progress analysis of crop stalk cutting theory and method. *Trans. Chin. Soc. Agric. Mach.* **2022**, *53*, 6, 1–20. [CrossRef]
13. Hang, H.D.; Wang, Y.X.; Tang, Y.Q.; Zhao, F.; Kong, X.F. Finite element simulation of sugarcane cutting. *Trans. Chin. Soc. Agric. Eng.* **2011**, *27*, 161–166. [CrossRef]
14. Meng, Y.M.; Wei, J.D.; Wet, J.; Chen, H.; Cui, Y.S. An ANSYS/LS-DYNA simulation and experimental study of circular saw blade cutting system of mulberry cutting machine. *Comput. Electron. Agric.* **2019**, *157*, 38–48. [CrossRef]
15. Xie, L.X.; Wang, J.; Cheng, S.M.; Zeng, B.S.; Yang, Z.Z. Optimisation and finite element simulation of the chopping process for chopper sugarcane harvesting. *Biosyst. Eng.* **2018**, *175*, 16–26. [CrossRef]

16. Cao, W.B.; Sun, W.L.; Niu, C.; Jiao, H.B.; Chen, B.B. Combed Safflower Picking Device Based on ANSYS/LS DYNA. *Trans. Chin. Soc. Agric. Mach.* **2018**, *49*, 123–131.
17. Souza, V.H.S.; Dias, G.L.; Santos, A.A.R.; Costa, A.L.G.; Santos, F.L.; Magalhães, R.R. Evaluation of the interaction between a harvester rod and a coffee branch based on finite element analysis. *Comput. Electron. Agric.* **2018**, *150*, 476–483. [CrossRef]
18. Ibrahmi, A.; Bentaher, H.; Hbaieb, M.; Maalej, A.; Mouazen, A.M. Study the effect of tool geometry and operational conditions on mouldboard plough forces and energy requirement: Part 1. Finite element simulation. *Comput. Electron. Agric.* **2015**, *117*, 258–267. [CrossRef]
19. Ahmadi, E.; Barikloo, H.; Kashfi, M. Viscoelastic finite element analysis of the dynamic behavior of apple under impact loading with regard to its different layers. *Comput. Electron. Agric.* **2016**, *121*, 1–11. [CrossRef]
20. Zheng, Z.J.; Kulasegaram, S.; Chen, P.; Chen, Y.Q. An efficient SPH methodology for modelling mechanical characteristics of particulate composites. *Def. Technol.* **2021**, *17*, 135–146. [CrossRef]
21. Afrasiabi, M.; Klippel, H.; Röthlin, M.; Wegener, K. An improved thermal model for SPH metal cutting simulations on GPU. *Appl. Math. Model.* **2021**, *100*, 728–750. [CrossRef]
22. Song, H.; Pan, P.; Ren, G.; Yang, Z.; Xu, J. SPH/FEM modeling for laser-assisted machining of fused silica. *Int. J. Adv. Manuf. Technol.* **2020**, *106*, 5–6. [CrossRef]
23. Hasanpour, A.; Istrati, D.; Buckle, I. Coupled SPH-FEM Modeling of Tsunami-Borne Large Debris Flow and Impact on Coastal Structures. *J. Mar. Sci. Eng.* **2021**, *9*, 1068. [CrossRef]
24. Du, M.; Wang, H.; Dong, H.; Guo, Y.; Ke, Y. Numerical research on kerf characteristics of abrasive waterjet machining based on the SPH-DEM-FEM approach. *Int. J. Adv. Manuf. Technol.* **2020**, *111*, 3519–3533. [CrossRef]
25. Liu, Q.T.; Qiu, Y.G.; Qing, S.L.; Wang, W.Z. Cutting Force Calculation of Sugarcane Stalk. *Trans. Chin. Soc. Agric. Mach.* **2006**, *37*, 89–92. [CrossRef]
26. Li, C.; Zhang, H.S.; Wang, Q.C.; Chen, Z.J. Influencing Factors of Cutting Force for Apple Tree Branch Pruning. *Agriculture* **2022**, *12*, 312. [CrossRef]
27. Wang, T.; Liu, Z.; Yan, X.; Mi, G.; Liu, S.; Chen, K.; Zhang, S.; Wang, X.; Zhang, S.; Wu, X. Finite Element Model Construction and Cutting Parameter Calibration of Wild Chrysanthemum Stem. *Agriculture* **2022**, *12*, 894. [CrossRef]
28. Liu, Y.; Huang, X.; Ma, L.; Zong, W.; Zhan, G.; Lin, Z. Design and Test of Static Sliding Cut Angle Constant Cutting Machine for Chain Oil Sunflower Harvester Header. *Trans. Chin. Soc. Agric. Mach.* **2021**, *52*, 99–108. [CrossRef]
29. Xun, X.L.; You, Y.; Wang, D.C.; Li, S.B.; Zhu, L.; Liao, L.L. Design and Experiment of Rotary Cutter Disc Type Flat Stubble Cutting Device for King Grass Harvester. *Trans. Chin. Soc. Agric. Mach.* **2022**, *53*, 112–124. [CrossRef]
30. Fu, Z.; Wang, D.; Li, W.; Huang, Y.; Zhu, R. Design and experiment of two-disc rotary mower of alfalfa. *Trans. Chin. Soc. Agric. Mach.* **2018**, *49*, 214–220. [CrossRef]
31. Liu, F.J.; Yang, X.J.; Fang, X.F. Design and experiment of chopper divice in sugarcane harvester. *Trans. Chin. Soc. Agric. Mach.* **2018**, *49*, 90–94. [CrossRef]
32. Kong, F.T.; Wang, D.F.; Shi, L.; Wu, T.; Chen, C.L.; Sun, Y.F.; Xie, Q. Design and experiment of disc-cutting picking device of castor. *Trans. Chin. Soc. Agric. Eng.* **2021**, *37*, 1–9. [CrossRef]
33. Wang, M.W.; Xue, Z.; Song, D.Q.; Zhang, L.F.; Zhang, J. Model analysis of cassavastalk cutter based on ANSYS. *J. Chin. Agric. Mech.* **2016**, *37*, 102–105+117. [CrossRef]
34. Hou, J.M.; Bai, J.B.; He, T.; Yang, Y.; Li, J.P.; Yao, E.C. Design and Experiment of Castor Dehulling and Cleaning Device with Double Curved Table. *Trans. Chin. Soc. Agric. Mach.* **2018**, *49*, 132–140. [CrossRef]
35. Ugwu, K.C.; Egwuagu, O.M.; Omoruyi, A. Determination of some mechanical and aerodynamic properties of castor fruits and seeds. *Int. J. Sci. Eng. Res.* **2015**, *6*, 659–666.
36. Lorestani, A.N.; Jaliliantabar, F.; Gholami, R. Physical and mechanical properties of castor seed. *Qual. Assur. Saf. Crops Foods* **2013**, *4*, e29–e32. [CrossRef]
37. Hou, J.M.; Bai, J.G.; Yao, E.C.; Zhu, H.J. Design and Parameter Optimization of Disc Type Cutting Device for Castor Stem. *ACCESS* **2020**, *8*, 191152–191162. [CrossRef]

Disclaimer/Publisher's Note: The statements, opinions and data contained in all publications are solely those of the individual author(s) and contributor(s) and not of MDPI and/or the editor(s). MDPI and/or the editor(s) disclaim responsibility for any injury to people or property resulting from any ideas, methods, instructions or products referred to in the content.